Wide and Small Angle X-ray Scattering on Talc Filled Polypropylene

Eirik Torbjørn Bakken

March 15, 2013

Abstract

Wide- and small-angle X-ray scattering has been performed on talc filled injection molded isotactic polypropylene to examen the preferred direction of molecules and the degree of orientation. Raster scanning was done over various part of the different samples to acquire the orientation gradient. It was discovered a clear sign of alignment for all samples, both from wide- and small-angle X-ray scattering. In particular it was discovered that the c-axis of talc tends to align itself perpendicular to the surface of the sample. The different samples also showed variation in the degree of orientation which can possibly be linked to the manufacturing process.

Contents

List of Figures

Chapter 1

Introduction

This report is a result of a project work at the Norwegian University of Science and Technology which is taken as a part of a degree in Master of Technology. The project is designed to let students get experience with working on a larger project, running for one semester, and learn to acquire and structure new knowledge in the form of a report, as is presented here.

This project was aimed at examining the polypropylene samples supplied by SINTEF. The goal was to see how the orientation of the scattering pattern from Wide Angle X-ray Scattering (WAXS) and Small Angle X-ray Scattering (SAXS) varied throughout the sample, and how this could be related to the orientation of the polypropylene. By performing a raster scan over the different samples, one could extract different parameters for analysis. This was done so one would have the basis for a further study of the material, where one could go in depth on the factors which were important and relevant for the microscopic structure. The overall goal for the study on these samples of polypropylene was to see how the polymers is oriented inside the sample, and in what way this is varying compared to where the polymer is injected, and compared to the surface normal. The continued work based on this project has been published in a scientific paper [1].

The experimental work was done at the X-ray group of the Institute of Physics at the Norwegian University of Science and Technology (NTNU) during four weeks in the period of June to August 2011. Associate professor Dag W. Breiby and phd. student Håvard Granlund supervised the project. Other persons involved in the project at the Institute of Physics were phd. students Jostein Bø Fløystad Morteza Esmaeili. It has in addition been included some results from a small-angle X-ray scattering measurement performed by Håvard Grandlund and Dag W. Breiby in November 2012. The samples were provided by SINTEF and were manufactured by injection molding. SINTEF was represented in the project by Per Erik Vullum and Erik Andreassen.

By studying this sample of polypropylene, it is hoped to gain more insight into the structure of the material. This material is one of the most important plastics in the world, with an estimated worldwide generated revenue of more than US $145 billion in the year 2019. The average growth the past eight years has been 4.4 % and

will likely be surpassed in the coming years [2]. With such an important material, it is clear that a good understanding of all its properties can have a large impact on an industrial scale. The fact that it is estimated that the material will still be of big importance in many years from now shows that a study of polypropylene is future-oriented.

The ability to make a large number of X-ray measurements of different parts of a sample has been possible due to the recent development in X-ray physics, and the establishing of a state of the art home laboratory at the NTNU. For mapping structural differences at sufficient resolution, one needs a beam with a spot size in the range of μm and also step motors which can move the sample with a resolution in the range of mm. The spot size can be focused using different kind of X-ray focusing techniques and the step motors can for example be made by piezo electric motors. The most important factor for mapping different kinds of gradients through the sample is the high resolution electronic detector, which have a small sampling time and fast readout time, preventing the experiment to be too time consuming. The fact that the computer industry is developing increasingly more powerful personal computers also makes it possible to analyze the large data samples in a reasonable time, without expensive high-performance computers.

This report will first give a short introduction to the material polypropylene with some relevant characteristics and a how the samples used in this project were manufactured. Then a description of the theory, the experiment and analysis will be given, to let the reader understand what kind of knowledge is needed to comprehend the result. This will be followed by the experiment section which will give a brief description of how the experiment was performed, and which areas of the samples were scanned. The last part of this report will contain a discussion and conclusion over the different kind of orientation and visibility plots for the different samples, and compare them to see the similarities and differences between the different samples.

Chapter 2

The Sample Analyzed

The sample analyzed for the wide angle X-ray scattering measurement was an isotactic polypropylene (iPP) sample provided by SINTEF, and was produced by injection molding. Talc had been added to the polypropylene for producing purposes. For the wide-angle X-ray scattering experiment, two different kind of samples were examined. One in the shape of a "dog-bone", and one in the shape of the front view of a house. They will further be be referred to as "dog-bone" and "house". The samples can be seen in Figure 2.1.

For the small-angle X-ray scattering experiment performed, nine different samples were used. They have the designation *EDXY*, where the two first letters, *ED*, is just referring to the sample type. The third letter, *X*, is referring to the mold temperature and is either *L* (low temperature), *M* (medium temperature) or *H* (high temperature). The last letter, *Y*, refer to the shear rate of the production of the sample. The shear rate is either *L* (low), *M* (medium) or *H* (high). The values for the low, medium and high temperature and shear rate are given in table 2.1

When neglecting the solidifying layer at the walls the shear rate, $\dot{\gamma}$, is given by

$$\dot{\gamma} = 3\frac{Q}{Ah}. \tag{2.1}$$

Q is the volumetric flow rate in m^3/s, A is the area of the cross section of the dog-bone neck and h is the smallest dimension of the cross section. The shear rate governs the injection speed of the melt and the pressure applied during solidification [3].

Table 2.1: The values for low, medium and high temperature and shear rate during the manufacturing of the samples.

	Shear rate	Temperature
Low	25 s^{-1}	20° C
Medium	150 s^{-1}	40° C
High	850 s^{-1}	65° C

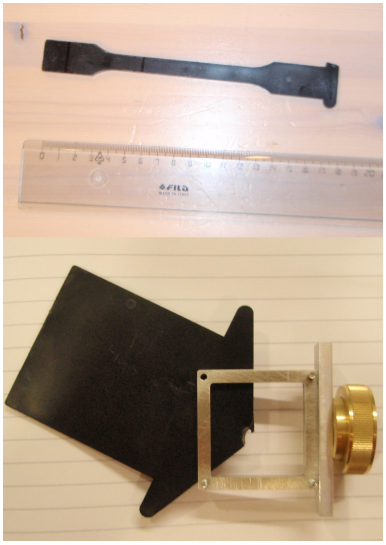

Figure 2.1: The two different samples being measured. The top is the one shaped as a "dog-bone" and the bottom is the one shaped as the front view of a house. At the top of the house roof the break off edge is visible. This is where the sample has been broken off from the rest injection mold, can be seen.

2.1 Polypropylene

Polypropylene is a material consisting of a repeating cell of propene, as described in Figure 2.2.

The material in this study is of the type isotactic polypropylene. This means that the methyl-groups all sit on the "same" side, shown in Figure 2.3 (a), and that the polymer is developing in a straight way, without any sharp bends. A nother type of polypropylene is shown in Figure 2.3 (b). This is syndiotactic polypropylene and will not be discussed further, but is shown to emphasize that polypropylene can from different kind of chains. Whether the polypropylene is isotactic or not has implications on the polymers ability to form crystals. Polypropylene with lower

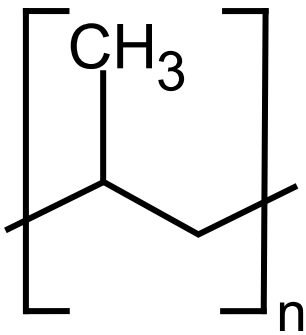

Figure 2.2: The repeating cell of polypropylene. n is a number in the range of ten thousands, symbolizing the repeating structure. A carbon atom with two attached hydrogen atoms is placed in each corner.

isotacticity, meaning more defects from a perfect isotactic chain, will form smaller crystals [4].

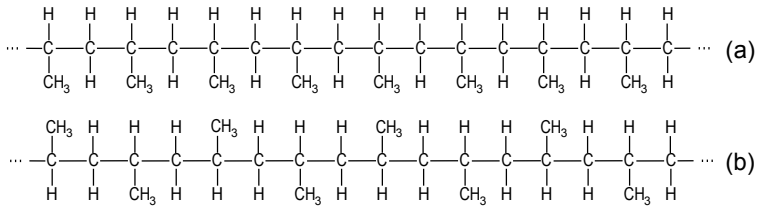

Figure 2.3: (a) shows isotactic polypropylene, while (b) shows syndiotactic polypropylene. Figure adapted from [5]

Isotactic polypropylene will crystallize in four different ways: α (monoclinic), β (hexagonal), γ (triclinic) and smectic. α is usually the far dominant form [6]. The structure of the unit cell in the α form is $a = 0.666$nm, $b = 2.078$nm, $c = 0.6495$nm, $\beta = 99.62°$ and $\alpha = \gamma = 90°$, where the chain is along the c-axis [7]. Which form the polypropylene crystallizes to depends on a number of factors as temperature [8] and shear strength [9]. Decreasing tacticity also has the implication of lower melting temperature and that more of the polypropylene will crystallize in the γ-phase [4].

The polypropylene samples used in this project were injection molded. This is a process where thermoplastics are forced in to a heated barrel where it is melted and mixed, typically by a revolving screw inside the barrel. This screw also forces the plastic forward from the intake towards the outlet where the mold is attached. The plastic is then injected to the mold cavity with a lower temperature, which cools and solidifies the plastic almost as soon as the mold is filled. Injection molding is the most used method to produce thermoplastic products [10].

2.2 Talc

Talc is a mineral with chemical formula $H_2Mg_3(SiO_3)_4$ and crystallizes in a monoclinic unit cell with parameters $a = 5.26$ Å, $b = 9.1$ Å, $c = 18.81$ Å and $\beta = 100°$ [1]. Talc has a number of effects when added to polypropylene. The ability to reinforce polymers [11] is one of the advantages, in addition reducing shrinkage and warpage, and reduce thermal expansion and the cycle time [1]. For these reasons talc have been added to the polypropylene samples. Better understanding of how the talc behaves inside the talc is thus a crucial step to understand the properties of polypropylene.

Chapter 3

Theory

The theory for X-ray scattering is based on the fact that electric charges will radiate electromagnetic waves when influenced by an incoming electromagnetic wave. This chapter will therefor start with giving a short description of radiation theory, and how this is influenced when the scattering comes from multiple charges situated on a periodic lattice. General assumptions and simplifications the theory is based on will be explained. In addition, the parameters the analysis uses will be explained, and some error analysis for measured means from a distribution.

3.1 Electromagnetic Waves and Photons

When dealing with X-rays, it is normal to make the two different descriptions, as is normal when dealing with electromagnetic waves. One can either adopt the classical view, and imagining an X-ray beam as a propagating wave in compliance with Maxwells equations, or regarding an X-ray beam as a stream of quantified photons. Which description is correct depends on which phenomenon is regarded.

When dealing with X-rays as electromagnetic waves, one adopts the formalism by describing the electric part of the wave with complex numbers:

$$\mathbf{E} = \mathbf{E}_0 \mathrm{e}^{i(\mathbf{k}\cdot\mathbf{r}-\omega t)}. \tag{3.1}$$

$\mathbf{k}$ is the wave vector of the electromagnetic beam, ω is the frequency, $\mathbf{r}$ the position vector and t is the time. The complex amplitude vector, $\mathbf{E}_0$, contains both information on the absolute amplitude of the wave, the phase of the wave and the polarization of the wave. Many materials have often refractive index close to unity in the X-ray regime, which means that an electromagnetic waves with these wavelengths considers the material almost similar to vacuum. This means that the polarization is perpendicular to the wave vector k, which follows from Maxwells equations for electromagnetic waves in vacuum. The real electric field is the real part of Equation 3.1. In this representation the electromagnetic wave is considered a plane wave, and this is normally a good approximation when dealing with X-ray scattering, because the wavelength is very small compared to the usual spot size. If one approximates the beam from the X-ray source like a Gaussian beam, the radius of curvature, R,

is given by:

$$R(z) = z\left(1 + \left(\frac{z_0}{z}\right)^2\right)[12]. \tag{3.2}$$

Here z is the distance from the beam center, and $z_0 = \pi W_0^2/\lambda[12]$, is the Rayleigh range, where W_0 is the beam width at the beam center, and λ is the wavelength of the beam. Since the beam width is in the order $\sim 10^{-4}$m, the wavelength is in the order of $\sim 10^{-10}$m and the distance from the beam center is in the order of ~ 1m the radius of curvature will be in the order of $\sim 10^5$m. The area illuminated by the X-ray beam is in the same order as the beam width, and it is therefore a good approximation to consider the incoming X-ray beam to be a planar wave when it is interacting with a sample because the radius of curvature is so large that the incoming beam will be planar over an area the size of the beam spot.

With these approximations, and considering a wave traveling in the x-direction and polarized in the z-direction in a Cartesian coordinate system, one can write the electric field of the incoming X-ray beam as:

$$\mathbf{E} = E_0 \sin(k_x x - \omega t)\hat{\mathrm{z}}. \tag{3.3}$$

Since it has been mentioned that X-rays can be regarded as particles, a short description will follow regarding the subject. When quantifying the electromagnetic wave, one is visualizing a particle called the photon with quantum energy $E = hf$. E is the energy, h is Planck's constant and f is the frequency of the electromagnetic wave. Viewing X-rays in this manner is important when considering the creation of characteristic X-ray spectra from the X-ray source and inelastic scattering as compton scattering, but will not be handled in more detail here, since it will suffice to know that photons exist to understand the work that has been done.

3.2 Scattering Theory

3.2.1 Fundamental Scattering Theory

The fundamentals of scattering theory lays on the fact that an electron will interact with an incoming electromagnetic beam, or photon, depending on which representation is most fitting. In most X-ray scattering experiments it is assumed that the scattering is elastic. This means that the scattered wave has the same wavelength as the incoming photon. When considering scattering from a single electron, one imagines that the incoming electromagnetic wave will act with a force on the electron, and hence start to accelerate it. This will again cause the electron to radiate according to

$$\frac{dP}{d\Omega} = \frac{e^2}{16\pi^2\epsilon}\frac{|\hat{\mathbf{r}} \times (\mathbf{u} \times \mathbf{a})|^2}{(\hat{\mathbf{r}} \cdot \mathbf{u})^5}[13]. \tag{3.4}$$

Which say that accelerated electric charges will be the source for an electromagnetic wave. Here $dP/d\Omega$ is the radiated power to an infinatly small steradian of a large sphere centered around the radiating particle. ϵ is the electric permittivity of the medium the electron is situated in, e is the electric charge, $\hat{\mathbf{r}}$ is the unit vector in radial directionvand $\mathbf{a}$ is the acceleration of the electron. $\mathbf{u} = c\hat{\mathbf{r}} - \mathbf{v}$ where c is the speed of light and $\mathbf{v}$ is the velocity of the electron . If one assumes that the incoming electromagnetic wave has an electric component on the form as seen in Equation 3.3, then, according to Newton's second law, the acceleration and velocity will be given by

$$\mathbf{a} = \frac{eE_0}{m_e}\sin(\omega t)\hat{\mathrm{z}} \tag{3.5}$$

$$\mathbf{v} = \frac{eE_0}{m_e\omega}\cos(\omega t + \alpha)\hat{\mathrm{z}}. \tag{3.6}$$

Here electrons located at $x = 0$ are considered. α is a constant depending on the initial condition and m_e is the electron mass. By including this in Equation 3.4 one gets that the radiated power per steradian is:

$$\frac{dP}{d\Omega} = \frac{e^4 {E_0}^2}{16\pi^2\epsilon m_e^2 c^3}\frac{\sin^2\omega t_r \sin^2\theta}{(1 - \frac{eE_0}{m_e\omega c}\cos\theta\cos(\omega t_r + \alpha))^5}. \tag{3.7}$$

$t_r = t - r/c$ is the retarded time, accounting for the fact that the signal need a finite time to travel the distance r. θ is the angle the radial unit vector forms with the z-axis. A single electron will thus give out electromagnetic radiation when accelerated by an electromagnetic wave. The fact that the scattered intensity goes as $1/m^2$, where m is the mass of the scattering particle, shows why only electrons are considered in x-ray scattering, and not protons. Protons have 1000 times the mass of an electron, and the scattering will therefore be very weak compared to the scattering from the electrons. However, when considering X-ray scattering one is usually not looking at scattering from a single electron, but from the sum of all electrons illuminated by the X-ray beam. This is because the electromagnetic waves interact in either a destructive or constructive way, depending on the phases of the waves. To understand this, it is necessary to first look at the scattering from a single atom. The scattering intensity is proportional with the absolute square of the atomic form factor, where the atomic form factor, f^0 is given by:

$$f^0 = \int \rho(\mathbf{r})\mathrm{e}^{i\mathbf{q}\cdot\mathbf{r}}d\mathbf{r}.[14] \tag{3.8}$$

where $\rho(\mathbf{r})$ is the charge density at position $\mathbf{r}$ and the scattering vector $\mathbf{q}$ is given by:

$$\mathbf{q} = \mathbf{k} - \mathbf{k}', \tag{3.9}$$

where $\mathbf{k}$ and $\mathbf{k}'$ are the incoming and outgoing wave vectors. When considering the scattering from multiple atoms, the sum over all the atoms atomic form factor is done, with the additional factor $\mathrm{e}^{i\mathbf{q}\cdot\mathbf{r}}$[15] to account for the fact that different atoms will spread with a different phase. As the intensity from the scattering from a single atom is proportional with the atomic form factor, the intensity from the scattering

from multiple atoms is proportional with the absolute square of the form factor, F, given by:

$$F(\mathbf{q}) = \sum_j f_j(\mathbf{q}) \mathrm{e}^{i\mathbf{q}\cdot\mathbf{r}_j} [14]. \tag{3.10}$$

Here the sum goes over all the different atoms involved, and $f_j(\mathbf{Q})$ is the atomic form factor of atom number j. If the atoms are situated at a lattice with lattice vector $\mathbf{R}$, then the form factor can be written as:

$$F(\mathbf{q}) = \sum_{\tilde{j}} f_{\tilde{j}}(\mathbf{Q}) \mathrm{e}^{i\mathbf{q}\cdot\mathbf{r}_{\tilde{j}}} \sum_n \mathrm{e}^{i\mathbf{q}\cdot\mathbf{R}_n}. \tag{3.11}$$

Here $\tilde{j}$ represent the atoms relative to each lattice point defined by $\mathbf{R}_n$,

$$\mathbf{R}_n = n_1\mathbf{a}_1 + n_2\mathbf{a}_2 + n_3\mathbf{a}_3. \tag{3.12}$$

$(\mathbf{a}_1, \mathbf{a}_2, \mathbf{a}_3)$ are the basis vectors of the lattice and (n_1, n_2, n_3) are integers. Since n is a large number and all the phase factors $\mathrm{e}^{i\mathbf{q}\cdot\mathbf{R}_n}$ will lie on the unit circle, the sum

$$\sum_n \mathrm{e}^{i\mathbf{q}\cdot\mathbf{R}_n} \tag{3.13}$$

will be 0 if

$$\mathbf{q}\cdot\mathbf{R}_n \neq 2\pi m \tag{3.14}$$

where m is an integer. This means that it is only scattering vectors, $\mathbf{q}$, equal to the reciprocal lattice vector, $\mathbf{G}$, that will interfere constructively, since the reciprocal lattice vector has the property

$$\mathbf{G}\cdot\mathbf{R}_n = 2\pi m \tag{3.15}$$

The condition

$$\mathbf{G} = \mathbf{q} \tag{3.16}$$

is called the Laue condition, and is also compliant with the Bragg law, stating

$$m\lambda = 2d\sin\theta. \tag{3.17}$$

Where m is an integer, λ is the wavelength of the incoming X-ray beam, d is the distance between the same type of planes in a crystal and θ is the angle of the incoming beam with the surface. The Bragg law follows from the same conditions as the Laue condition that the scattered waves all have to be in face. In the Bragg law one imagines parts of the incoming wave to be reflected at each layer of scattering planes, and that the distance between each plane has to be on the form of Equation 3.17 for the outgoing wave to be in face. The Bragg law will not be explained further, but is shown because it is a famous result, and some people are more comfortable with looking at the scattering from the view of real space, as opposed to the Laue condition which looks at it from reciprocal space. It is therefore added to emphasize that it is no difference between these to methods to look at the scattering condition.

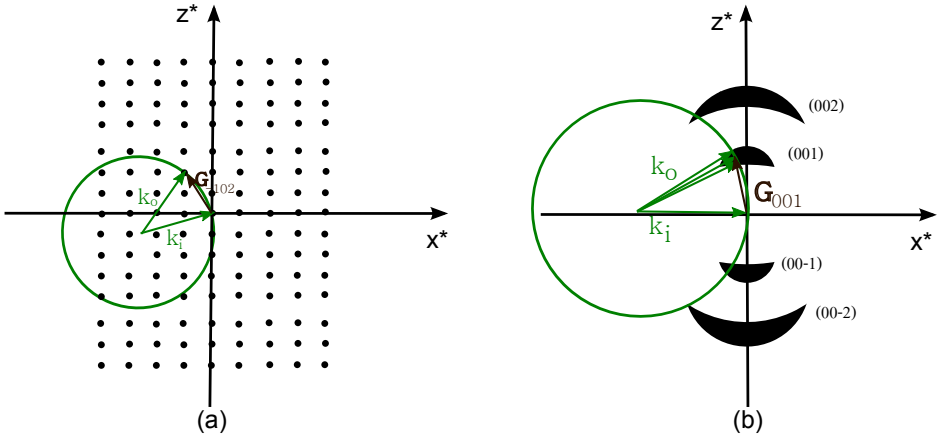

Figure 3.1: a) A cross section of a perfect crystal in reciprocal space. Each point represents a set of scattering planes. $\mathbf{k_i}$ is the incoming wave vector ending at the origin. The Ewald sphere is a sphere with the incoming wave vector as radius. Any reciprocal lattice point intersecting the Ewald sphere will fulfill the scattering criterion and an outgoing wave vector $\mathbf{k_o}$ will follow the path as indicated. $\mathbf{G_{-102}}$ is the reciprocal lattice vector that is equal to the scattering vector $\mathbf{q}$ in this particular case. b) Reciprocal space of a non-perfect crystal. Different crystals are rotated with respect to each other along an axis normal to the ones shown. This will spread out the single points (001), (00-1), (002) and (00-2) over an area in reciprocal space. The scattering condition can therefore be fulfilled for different incoming wave vectors, and the outgoing scattering vector can have multiple directions, not just forming a single spot, but lobes, or in a powder; rings. This is illustrated by the three outgoing wave vectors all fulfilling the same scattering conditions.

3.2.2 Scattering From a Non-Ideal Crystal

The Laue conditions can be described by looking at the Ewald sphere in k-space, as shown in Figure 3.1 (a). Here, all points describe a reciprocal lattice point, and those points that are situated at the sphere created by the incoming wave vector $\mathbf{k}$, will fulfill Laues condition. For a perfect crystal only, a few points will fulfill the condition, depending on the orientation of the crystal with respect to the incoming beam. If one however have a material without perfect crystallinity, the lattice points in reciprocal space will be smeared out over an area. This is demonstrated in Figure 3.1 (b). Since each point has been smeared out in reciprocal space more points will be able to fulfill Laues condition. This is seen in all three dimensions, thus smearing out the single point over an area in reciprocal space. This means that the scattered beam will not be focused in one single point, but will be smeared out in lobes on the detector. In the extreme case where the material being radiated is a powder, the reciprocal points will be a perfect sphere around the origin in reciprocal space and the diffraction signal will be a circle around the incoming beam.

Applying this to a material as polypropylene it could be expected that reciprocal lattice will be smeared out, similar to Figure 3.1 (b). Since polypropylene consist of a very long chain of molecules it would be believed that one direction would be

preferred over the other directions. The molecules will however likely be somewhat tilted with respect to each other and thus not creating a perfect crystal. When then doing a scattering experiment one could expect to not see perfect spots, but lobes centered around the incoming beam.

3.3 Theoretical Background for the Parameter Used in the Analysis

There were a number of different parameters analyzed from the diffraction pattern registered by the detector. Figure 5.1 and 3.2 shows an ordinary diffraction pattern and how it was analyzed by the computer program created by Håvard Granlund[1]. The analysis was done by selecting a q-range of interest on the detector image and then fitting it to a Gaussian curve on the form

$$G = A \cdot \mathrm{e}^{\left(\frac{(\theta-\chi)^2}{2d^2}+\frac{(\theta-\chi-180)^2}{2d^2}+\frac{(\theta-\chi+180)^2}{2d^2}\right)} + B. \tag{3.18}$$

Here θ is the angle of the peak of the signal, χ is the azimuthal angle on the detector image, A is the amplitude, B is the background and d is the full width at half maximum (FWHM) of the peak. From this fit one can draw out a number of parameters. The orientation of the scattering signal lies in the parameter θ and can be used for analyzing the preferred direction of the scattering signal.

The visibility was in this project defined as

$$V = \frac{A}{A+B}, \tag{3.19}$$

where A is the amplitude of the gaussian fit, as before, and B is the background, as marked in Figur 3.2. The visibility can say something about the degree of orientation, where a high visibility and a sharp peak would usually mean high order of orientation because then more crystals would scatter in the same direction, which means they have the same orientation. Although a high visibility in itself is not a measurement of degree of orientation because the visibility can still be high in an material if the width of the peak is very large. This can for example happen for a material with strong scattering, but with a certain forbidden orientation. The scattering amplitude can then be generally large, except in a single region where it will be no scattering at all, thus making the visibility large although the degree of orientation is low. The peak width of the scattering signal did however not look alarmingly large in the measurements done in our experiment, and it can therefore be safe to say that a high visibility at least indicates a higher degree of orientation than a low visibility.

The SAXS data was analyzed by a program created by Oliver Bunk[2]. The detector image was divided in to 16 sections, as shown in Figure 3.3. The q-area of

[1]Institute of Physics, NTNU

[2]Paul Scherrer Institute

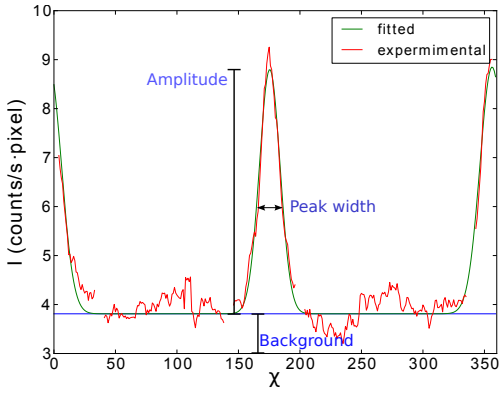

Figure 3.2: A typical signal from the detector. The angle χ is the angle around the detector image counter clockwise. The red line is the experimental data, while the green is the fitted curve. The background, amplitude and peak width (FWHM) are indicated on the figure.

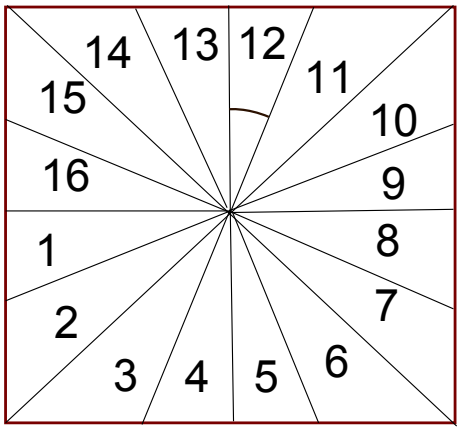

Figure 3.3: In the SAXS analysis the detector image was divided in to 16 sections, marked 1-16. The different pixel values for each q-value in each section was integrated, as marked by the brown line in section 12, to get the direction the scattering signal was strongest.

each sections was integrated to see which direction each of the scattering signals were strongest, for the different q-values. The program also analyzed a number of other parameters based on the fourier components of the signal, but this is outside of the scope of this report, and is therefore omitted.

3.4 Error Analysis

Because it is in some cases necessary to calculate the mean of some variables it has been added a small section on error analysis of sample means. The Central Limit Theorem says that if the mean, $\bar{X}$, of a random sample of size n taken from a population with mean μ and finite variance σ^2, then the variable

$$Z = \frac{\bar{X} - \mu}{\sigma/\sqrt{n}} \tag{3.20}$$

will be normal distributed with mean zero and standard deviation one, as $n \rightarrow \infty$[16]. For a sample size over 30 the Central Limit Theorem is a good approximation. This is however based on the fact that the standard deviation of the distribution the samples are taken from is known. If this is not the case the sample variance

$$S^2 = \frac{1}{n-1}\sum_{i=1}^{n}(X_i - \bar{X})^2 \tag{3.21}$$

can be used instead. The variable

$$T = \frac{\bar{X} - \mu}{S/\sqrt{n}} \tag{3.22}$$

will then be t-distributed with $n-1$ degrees of freedom. This has a restriction that the samples has to be originally drawn from a distribution with normal population. It can however be shown that the t-distribution is a good approximation for populations with a similar distribution shape as the normal distribution [16].

T can further be used to construct a 100(1-α)% interval of confidence. Here α is a value between 0 and 1. A 100(1-α)% interval of confidence for the true mean value μ is constructed as:

$$\bar{x} - t_{\alpha/2}\frac{s}{\sqrt{n}} < \mu < \bar{x} + t_{\alpha/2}\frac{s}{\sqrt{n}}. \tag{3.23}$$

$t_{\alpha/2}$ is the t value leaving an area under the curve equal to $\alpha/2$ to the right. $\bar{x}$ is the measured mean, and s is the estimator for the sample variance, as given in Equation 3.21. The true mean value μ will, with 100(1-α)% probability, be inside of this interval.

Chapter 4

Experimental Procedure

4.1 WAXS Measurement

The experimental set up for the WAXS measurement is shown in Figure 4.1. It was used a molybdenum source, which has characteristic X-ray emission lines at wavelength 0.7 Å. The width of the X-ray beam was measured to be around 0.2 mm. This was achieved with a series of slits placed before the sample holder. The sample holder was placed on a Newport linear stage stepper motor which made it possible to move the sample with below µm precision. Following the sample holder, a Dectris 1M Pilatus detector was placed, which recorded the scattering signal by counting each photon hitting the detector and stored it in a matrix, depending on which pixel on the detector the photon hit. The experiments were performed by exposing the sample for the X-ray beam for a time between 60 and 200 seconds, depending on which sample was being measured, and at the same time measuring the scattering with the detector. After each exposure time, the sample was moved in either x or y direction and a new recording of the scattering was started. In this way the hole, or parts, of the sample was scanned. The entire experiment was automated, and controlled from a computer.

All the different scans done one the samples are shown in Figure 4.2 with scan number, to make it easier to separate them.

4.2 SAXS Measurement

The small-angle X-ray scattering measurement were performed at the Swiss Light Source (SLS) at the Paul Scherrer Institute in Switzerland. The SLS is a third generation synchrotron light source, which can produce photons with energy up to 2.4 Gev [17]. The synchrotron produces photons by accelerating electrons in a magnetic field. The electrons are first accelerated in a linear accelerator. Second the electrons are transfered to a booster synchrotron, which give them the desired kinetic energy. After the electrons has reached its final kinetic energy, they are put in to the storage ring. Here they will be exposed to various alternating magnetic fields in order to give off electromagnetic radiation.

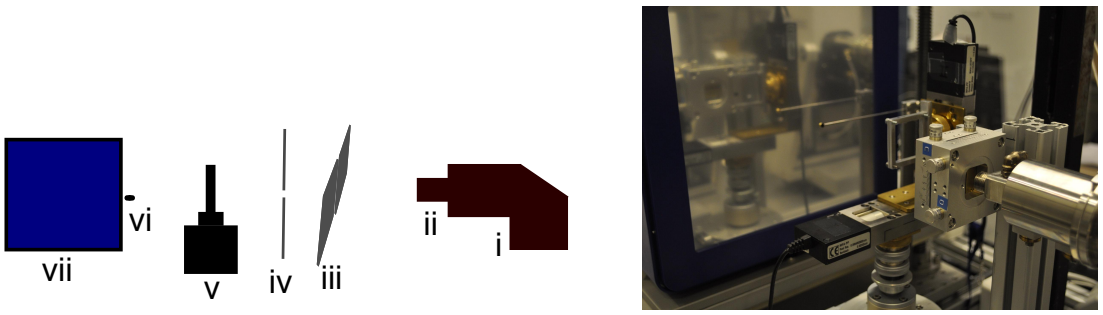

(a) (b)

Figure 4.1: The experimental set up for the experiment. a) Graphical view of the set up. i: Molybdenum X-ray source, ii: X-ray focusing optics, iii: vertical slits, iv: horizontal slits, v: sample holder with step motors, vi: beam stop, vii: detector. b) Real image of the experimental set up.

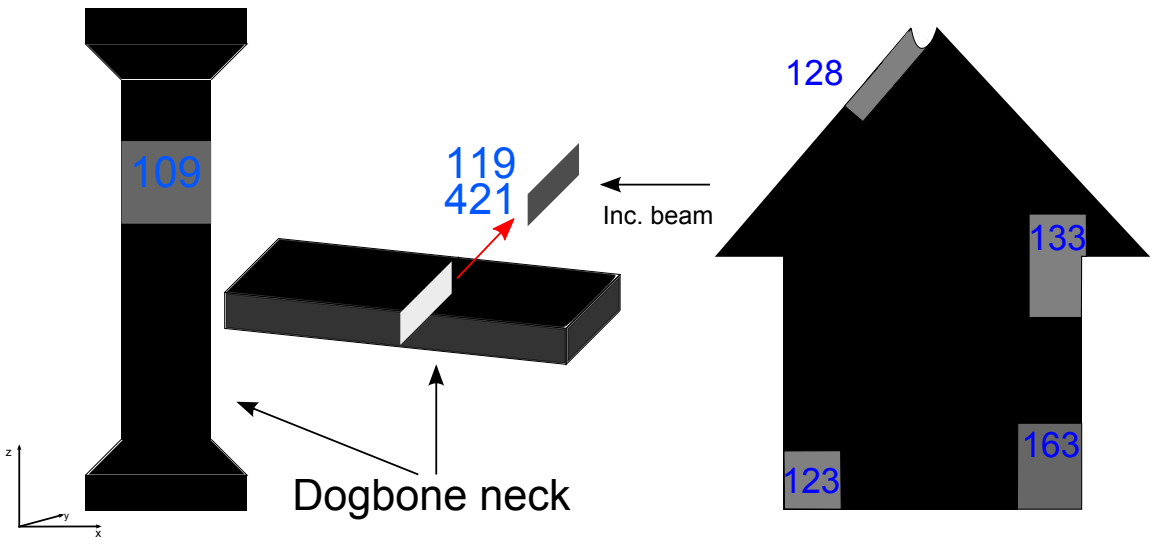

(a) (b)

Figure 4.2: The different scans done on the two samples. (a) The scans done one the dog-bone with corresponding scan number. A coordinate system has been added to the dog-bone sample to ease the discussion. (b) The scans done on the house, with corresponding scan numbers.

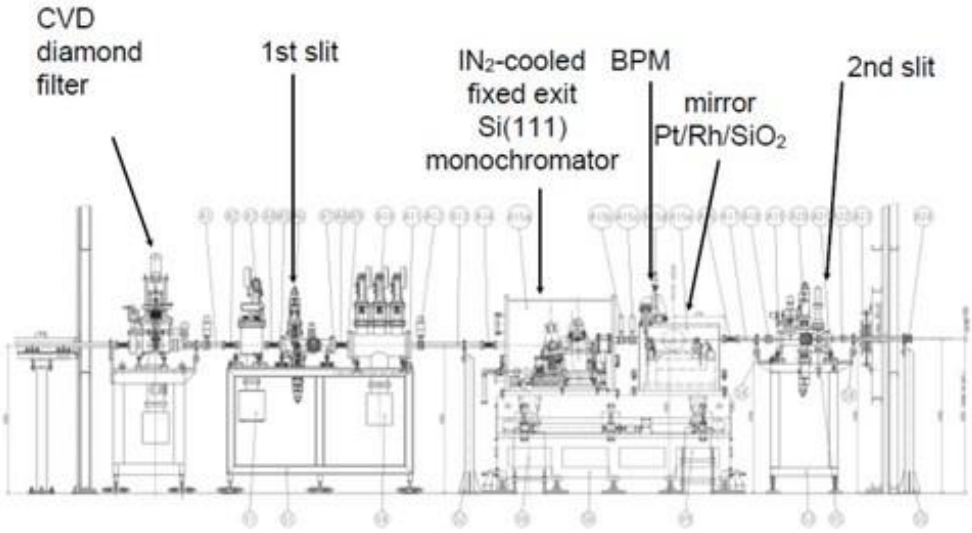

Figure 4.3: The first part of the experimental set up for the SAXS measurement. The X-ray beam is entering from the left. In addition to the elements marked, more slits and a fast shutter was placed to the right of where the figure ends. Figure adapted from the Swiss Light Source website [17]

When performing SAXS measurements it is necessary with a highly collimated beam with very low beam width and high flux. This is because the measurements done with a wide and uncollimated beam will be influenced by larger areas of the sample. If it is variation within the sample then the scattering signal will be influenced by multiple scattering regions, and the signal will be much more difficult to analyze. All this is possible with a synchrotron. The fact that a synchrotron also generally has a higher flux than a typical home laboratory makes it preferable to perform such measurements at the SLS.

The first part of the experimental set up is given in Figure 4.3. After this the sample was placed on stepping motors, followed by a 7 meter long evacuated flight tube. The detector used was a Pilatus 2M detector.

Chapter 5

Results

This chapter will present the result of different scattering experiment on the different samples. For the WAXS experiments two different kind of plots are given for each scan. One is showing the orientation of the scattering pattern the color of the plot is giving the direction of the scattering pattern as indicated by the color wheel, while the gray scale is symbolizing the degree of orientation. Higher gray scale means lower degree of orientation. The other plot gives the visibility of the scattering signal. The visibility is a measure of the degree of orientation, and is hence also included in the first plot. It was however chosen to include both plots, because it is easier to read the visibility plot when it comes to degree of orientation. Two typical images from the WAXS experiment recorded by the detector is shown in Figure 5.1. Different rings can be seen on the image, which comes from different satisfactions of the scattering criterion as discussed in section 3.2. The scattering signal is however not isotropic but concentrated around a peak value.

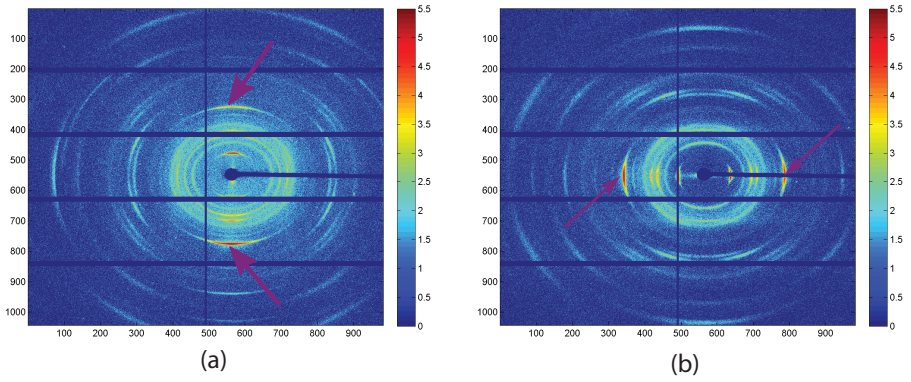

Figure 5.1: Two typical WAXS images from the polypropylene samples. The color bar indicates the number of counts on a logarithmic scale. a) is from scan 119 and b) is from scan 109. One can see a number of different diffraction circles, which has the intensities focused at specific areas of the circle. This indicates that it is some kind of preferred direction, and not a random orientation. The rest of this analysis will be focused on the ring marked with the purple arrows. The straight dark blue lines come from the fact that the detector consist of different modules, and also the beam stop.

The large number of rings could make it possible with a deep analysis of the the images, where the different rings where analyzed separately to get more informations on the different crystalline axes and how oriented they were with respect to each other. It was however noted that, to eye measurement, the alignment of many of the different rings all followed the same pattern in such a way that when the bright diffraction pattern marked with the purple arrows in Figure 5.1 rotated, the rest of the rings rotated an equal amount in the same direction. The development of the direction of the scattering signal would therefore be very similar between the rings. Although the visibility would be different for the different diffraction patterns, it was decided to only make an analysis of the development of the ring marked with the purple arrows. This ring is the $(hkl) = (006)$ reflection of talc [1]. An important fact is that the scattering signal is not entirely symmetric. The top diffraction pattern marked by the purple arrow in Figure 5.1 (b) is weaker than the bottom diffraction pattern marked by the other purple arrow.

5.1 Scan of Dog-Bone Neck

The results from the scan of the dog-bone neck in the xz-plane, marked with scan number 109 in Figure 4.2 (a), are given in Figure 5.2 and 5.3.

The orientation of the scattering signal is clearly aligning itself perpendicular to the edge of the sample, and the orientation is strongest closer to the edge, as indicated by the brightness of the color and the high visibility. The orientation is also in general stronger at the right part of the sample compared to the left. Closer to the center the orientation breaks down, as indicated by the black color, which indicates that there is no preferred orientation.

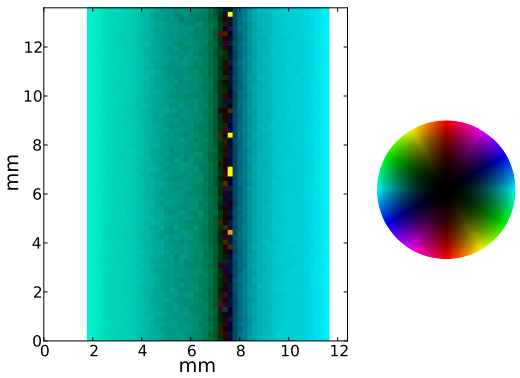

Figure 5.2: The orientation of the scattering pattern from scan 109. The diffraction pattern is clearly aligned with the edges of the dog-bone. Towards the center, one can notice that the color turns black, which means that there is no preferred alignment. This does however not happen at the symmetric center of the dog-bone neck

When comparing the two different plots, it is noticed that the plotting parameter is not symmetric around the center of the sample, but shifted to the right. It can also be seen that the orientation and visibility are clearly stronger in the right

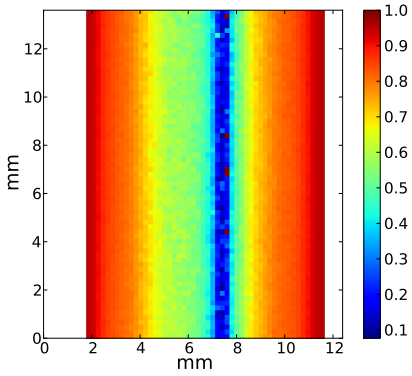

Figure 5.3: The visibility of the diffraction pattern from scan 109. The visibility is highest at the edges of the sample, and slowly decreasing towards the center. This is consistent with Figure 5.2, where there was no preferred orientation at the center, which was located to the right of the symmetric center of the dog-bone.

part of the sample. Both parameters are also strongly affected by the edge of the sample. This is especially visible in Figure 5.3 where the parameter value is highest towards the edge. From the visibility plot, it is noticed that the plotting parameter stays high (the red area) for roughly the same distance inwards in the sample for both sides, but the visibility in the right part drops down much quicker to a lower value compared to the left part.

5.2 Scan of Dog-Bone Neck Cross Section: High Resolution

The plots for scan 119, where the incoming X-ray beam was incident at the cross section of the dog-bone neck, as illustrated in Figure 4.2, are given in Figure 5.4 and 5.5. This scan was done with high resolution, to see more details among the different part of the sample.

Figure 5.4 shows the orientation of the diffraction pattern in the sample. It is clearly strongly affected by the edges of the sample, as indicated by the bright colors. The orientation goes from a gradual alignment perpendicular to the left edge to be oriented perpendicular to the top or bottom edge. The orientation is symmetric along the horizontal center line with no special feature standing out compared to the rest of the sample.

The visibility shown in Figure 5.5 is high throughout the sample, and only dropping at the center of the sample. The visibility is large in the middle of the sample, and falling a little above and below, which forms an area stretching out to the corners. This feature can not be observed in Figure 5.4, and this indicates that the reason for this formation might not be directly caused by the orientation of the molecules. The edges at the top and bottom seems to have a lower visibility than what it is a small distance towards the center of the sample. This is different than what can be observed in Figure 5.3, were the visibility were strongest at the edges. The left edge

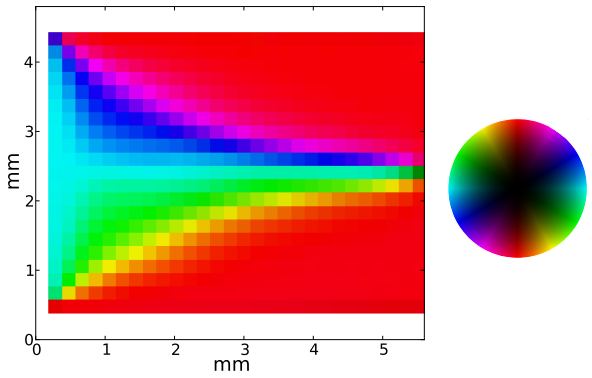

Figure 5.4: The orientation of the scattering signal from scan 119. There is a strong alignment toward the edges of the sample, indicated by the red and light blue colors. There is also a gradual transition between the vertical edge and the horizontal edges.

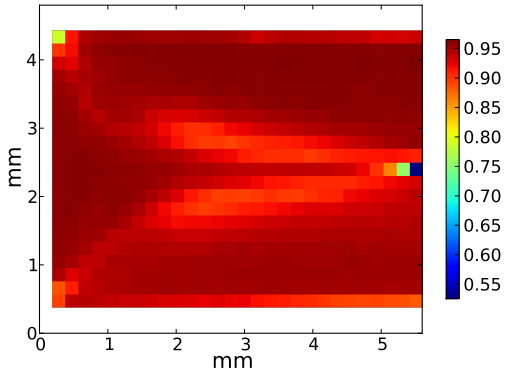

Figure 5.5: The visibility from scan 119. It is a high visibility throughout the sample. The only exception is at the very center, where the visibility drops to 0.55. Since the visibility is high, the amplitude of the scattering signal is high compared to the background. This can indicate a high degree of orientation, because the scattered signal is not spread out over a ring, but concentrated at the peaks. One can also see that it seems like the visibility is higher in the top part of the sample, compared to the bottom part.

does however have higher visibility compared to the neighboring region.

5.3 Scan of Dog-Bone Neck Cross Section: Low Resolution

A low resolution scan over the entire cross section of the dog-bone neck, marked as scan number 421, is shown in Figure 5.6 and 5.7. Both of these plots have a white marking at the top right corner, which is caused by the sample holder, and not the sample itself.

The orientation of the scattering signal shown in Figure 5.6 is clearly affected by the edges. The orientation of the scattering is gradually turning from being perpendic-

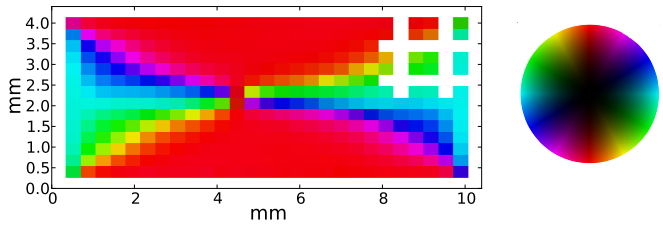

Figure 5.6: Orientation of the scattering signal in scan 421. The orientation of the scattered signal is aligning itself perpendicular to the edges. This is similar to both Figure 5.2 and Figure 5.4. The development of the alignment of the scattered signal is not symmetric to the sample geometry. This is consistent with Figure 5.2 and 5.3 where it was observed that the signal symmetry was shifted to the right.

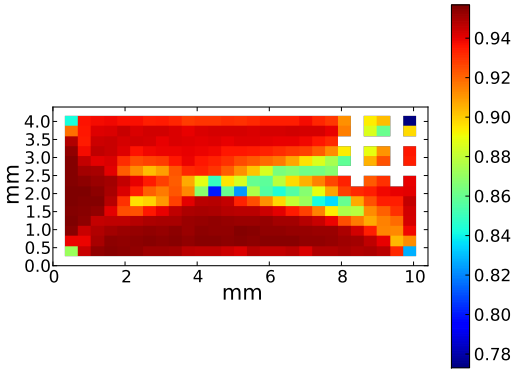

Figure 5.7: The visibility of the scattering signal in scan 421. The visibility of the scattering signal is high throughout the sample. The left part of the sample has a clearly higher visibility than the right part. When comparing to the high resolution scan in Figure 5.5, they are clearly consistent with eachother. The visibility symmetry is clearly shifted to the left of the center.

ular to the top and bottom edges, to be perpendicular to the left and right edges, as seen in Figure 5.4. It can be seen that the orientation is roughly symmetric around a horizontal line through the sample center, but it is not symmetric around a vertical line through the center. Here, it is shifted to the left of the sample, and this is in agreement with the decentering seen in Figure 5.2 and 5.3. The reason why the decentering in the cross section is to the left, and in the dog-bone neck to the right, is because the incident beam was in the positive y-direction for the dog-bone neck scan, while it was in the negative z-direction for cross section scan. The decentering is therefore located at the same place in the sample, and not caused by other effects.

In Figure 5.7 the same kind of development where a horizontal V-shape stretches out from the center towards the corners in both directions can be seen as observed for the orientation plot. An interesting observable is that the value of the visibility is not the same on both sides. It is clear that the visibility is higher in the bottom part of the sample, compared to the upper part, and the left part also has a higher visibility compared to the right part.

5.4 Scan of Bottom Corners of House Sample

The results for the scans around the two bottom corners of the house, marked as scan number 123 and 163, are presented in Figure 5.8 and 5.10. The scan of the right corner is of a larger length scale, but with the same resolution.

The orientation plotted in Figure 5.8 is done with a different method than the other orientation plots. This was done to emphasize bending from the vertical edges towards the corner, and the discontinuity in direction above the bottom edge, where the changing of the orientation is much larger than the resolution of the scan. This was also observed by looking at the image data from the detector. The choice of this kind of plot is also based on the factor that this gives a somewhat better information on the strength of the orientation in this case, where the length of the bar symbolizes how strongly that area is oriented. The orientation is strong along the edges, but decreases significantly when one moves inwards in the sample. Close to the bottom it can be observed that the development of the direction seems to have a discontinuity in the horizontal component of the orientation gradient. The orientation of the scattering signal have a large change over a small distance in the vertical direction. This effect is shown in Figure 5.9. It does not seem to be any major differences between the to corner areas of the sample with regard to the orientation.

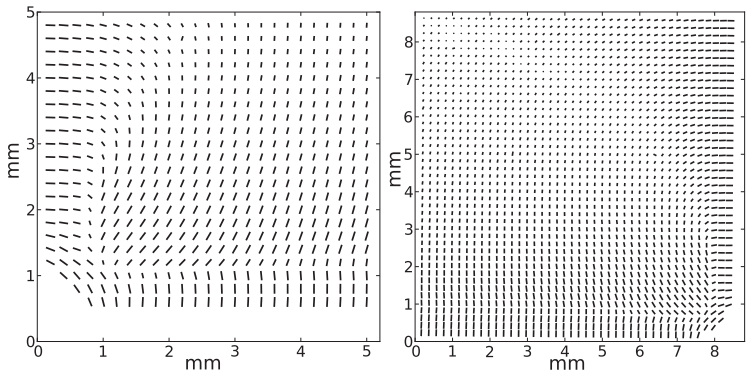

(a) (b)

Figure 5.8: The direction of the scattering signal of from the two bottom corners of the house. a) Scan 123, b) scan 163. It is a rather strong orientation in both corners, where the length of the lines symbolizes how strong the orientation is. One can clearly see that the orientation is directed towards the bottom left and bottom right corner of the sample in scan 123 and scan 163. At the edges the scattering signal is orienting itself perpendicular to the surface, except at the bottom left/right corner, where the scattering signal is aligning itself parallel to the edge. Close to the bottom a discontinuity of the horizontal component of the directional gradient is visible.

The visibility of the two corner areas, as shown in Figure 5.10, also looks to be fairly similar, as it did for the orientation. The visibility is clearly strongest at the

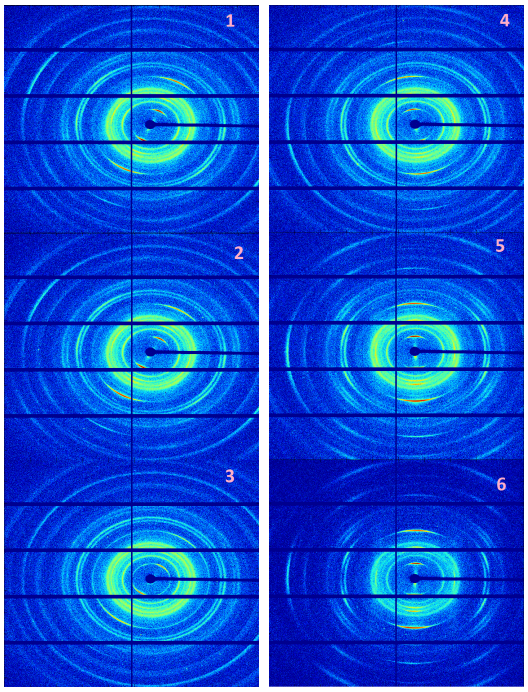

Figure 5.9: Column of images near the bottom of the sample in scan 123. A sudden discontinuity between image 3 and 4 by looking at the innermost diffraction pattern.

edges, and decreasing inwards in the sample. It is observed that close to the corners a region of low visibility is sliding under a part of high visibility near the bottom. This can be seen for both corners, but the effect looks to be strongest for the lower left corner in scan 123.

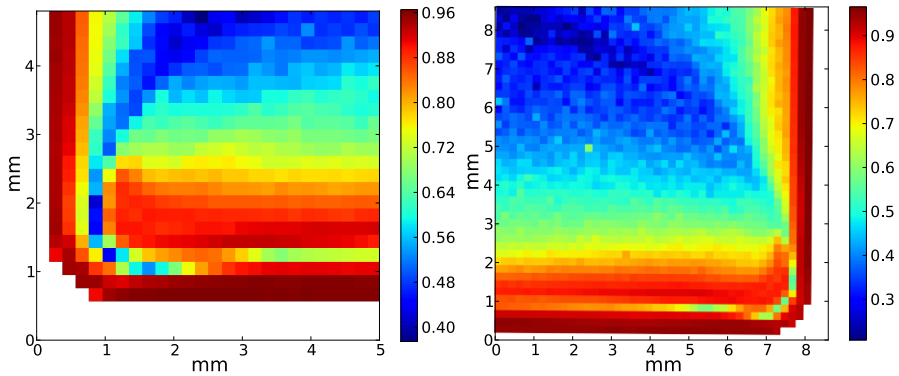

(a) (b)

Figure 5.10: The visibility of the two bottom corners is strongest toward the edges, and decreasing towards the center of the sample. It can be noticed that it is a small area of low visibility sliding between two areas with high visibility near the bottom.

5.5 Scan of Area Between Wall and Roof of House

The orientation and visibility of the section of the house around the area of the house wall and house roof, as indicated by scan number 133 in Figure 4.2 is shown in Figure 5.11. Both figures show much of the same tendencies, where the plotting parameter is highest towards the edge, and decreasing inwards. An effect at about 8.5 mm and 13 mm in vertical direction, where it is seen a distinct line in both plots, is observed. This is an area where the sample thickness was reduced. The thin part was in the area [8.5 mm,13 mm]. In Figure 5.11 (b), the visibility falls down more rapidly in the area of low thickness, but the maximum value looks to be the same as the maximum value in the area with thicker thickness.

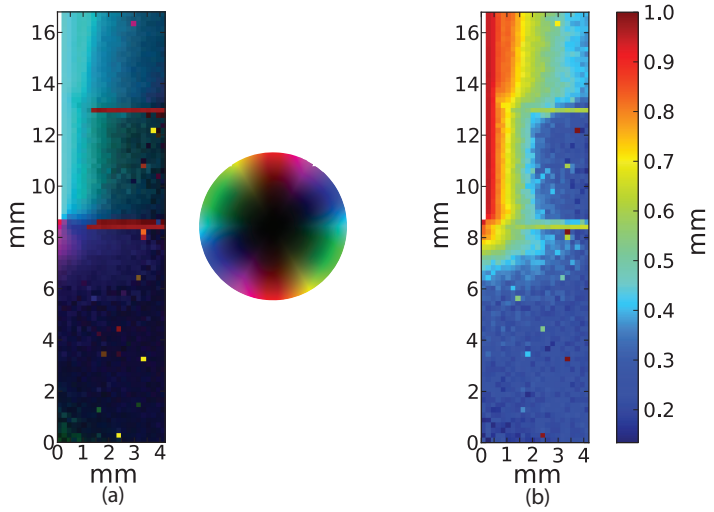

Figure 5.11: The orientation and visibility of scan 133. a) The orientation of the diffraction pattern is strongly oriented perpendicular to the surface edge. It is however quickly becoming weaker as one moves inwards the sample, as indicated by the fact that the colors become darker. Red horizontal lines at 8.5 mm and 13 mm in vertical direction is caused by the fact that this area was a transition between a high to a slightly lower thickness of the sample. b) The visibility is clearly highest towards the outer edge, marked with white color in the plot. One can note that the visibility drops off quicker in the thin part of the sample, between 8.5 mm - 13 mm in vertical direction.

5.6 Scan Around Breaking Area of House

The results of the analysis of scan 128, which was over the top of the roof of the house, are given in Figure 5.12 and 5.13. Figure 5.12 shows that the orientation of the scattering sample is rotating as it follows the breaking edge, which is at the lower part of the scan. The scattering signal is therefore not aligning itself either perpendicular or parallel to the edge of the breaking point, but rather both, depending on where along the edge one looks. It is thus no specific alignment with the edge, but breaking of the polypropylene sample does clearly not form stochastic

variations in the direction. Along the vertical edge the orientation is slightly tilted compared to the edge and not aligning itself perpendicular to the edge surface before a little distance inside the sample. This has not been observed to the same degree in the previous scans, where the alignment has always been almost perpendicular to the edge. The strength of the orientation can also seem to be slightly lower at the edge, than a small distance inside.

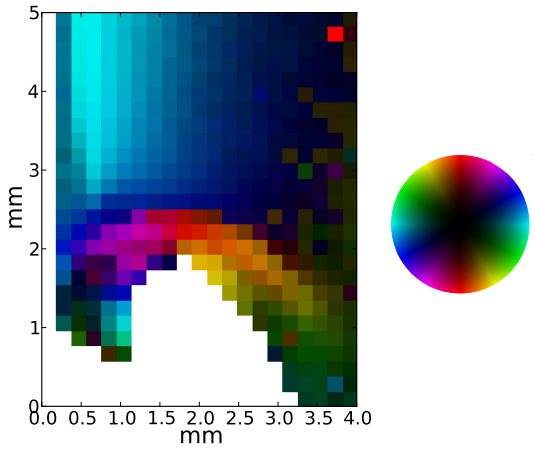

Figure 5.12: Orientation plot of scan 128. The orientation of the scattering signal shows that the alignment at the vertical edge is slightly weaker compared to a small distance inside the sample, and also tilted compared to the surface. At the point where the sample has be broken loose from the mold, forming a upside down U at the bottom, the alignment is starting, at the right part of the break of edge, on the green part of the scale. The orientation is then turning clockwise as one follows the edge at the break off point.

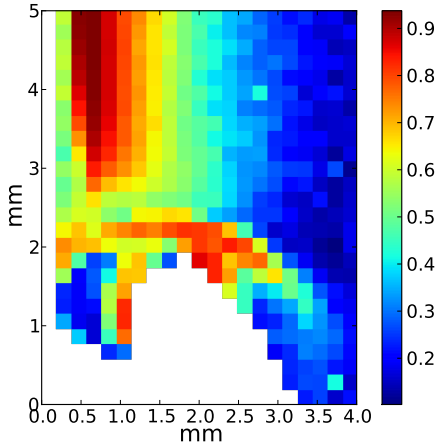

Figure 5.13: The visibility of the scattering pattern in scan 128. The visibility is highest a small distance from the vertical edge, which match the pattern seen in Figure 5.12. Along the breaking point, the visibility varies between 0.3 and 0.8. This indicates that how the breaking occurs can have significant effects on the macroscopic scale. At the end of the peninsula, at the bottom left, the visibility is less than to the right and above.

The visibility shown in Figure 5.13 shows that some parts around the breaking point forms regions with high visibility, while other regions have low visibility. At the vertical edge one can see that the visibility is not strongest along the very edge, but is increasing a small distance inwards. The area with high visibility coincide with the part at the orientation plot with a bright blue region, a small distance from the vertical edge, marking a high degree of orientation.

5.7 Small Angle X-ray Scattering

A typical diffraction signal from the ED-samples is shown in Figure 5.14 (a), while Figure 5.14 (b) shows how the signal varies as a function of q for 16-different sections on the detector. One can see that there are many different diffraction peaks in the signal. For the further analysis, the q-area of q = 0.002-0.007 Å^{-1} was used, as marked in Figure 5.14 (b).

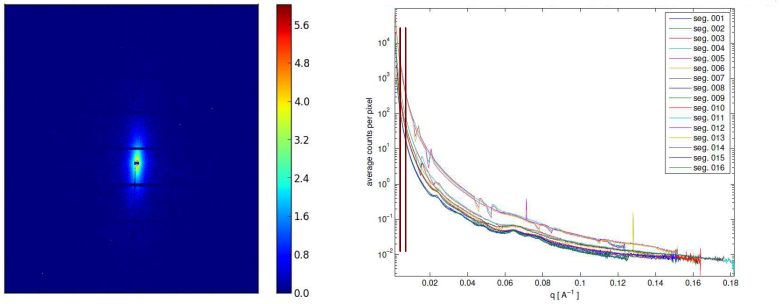

(a) (b)

Figure 5.14: a) A typical diffraction image of the small angle X-ray scattering experiment. It is clearly a direction of the diffraction pattern centered around the beam stop. b) The detector image has been sectioned in 16 sections and the diffraction pattern has been integrated up for each q-value. The area between the two red bars represents the q-area which was analyzed.

The orientation of the scattering signal for low q for small-angle X-ray scattering is given in Figure 5.15. It is highly visible that the scattering signal also for SAXS measurements are oriented perpendicular to the edge, in the same way as for WAXS. The measurements are done on different samples manufactured under different shear rates and different temperatures. The figure shows many similarities, but also differences. Those samples manufactured with high shear rate have a feature to the right of the sample center, which is marked with a black ring in Figure 5.15 (i). Here, it is visible that a dark blue area turn upwards. This is visible for all samples with high shear rate, but only on one of the sides. This feature is not visible for low or medium shear rate, and one can not find it in Figure 5.15 (a) as one should expect if this feature would happen for lower shear rates, since it is in the same region as where the feature is observed for high shear rates. The black line in Figure 5.15 (d) shows the area where a one-dimensional line scan of the orientation

were done. This was done to see more of the development of what happened in the region the black rings are marking.

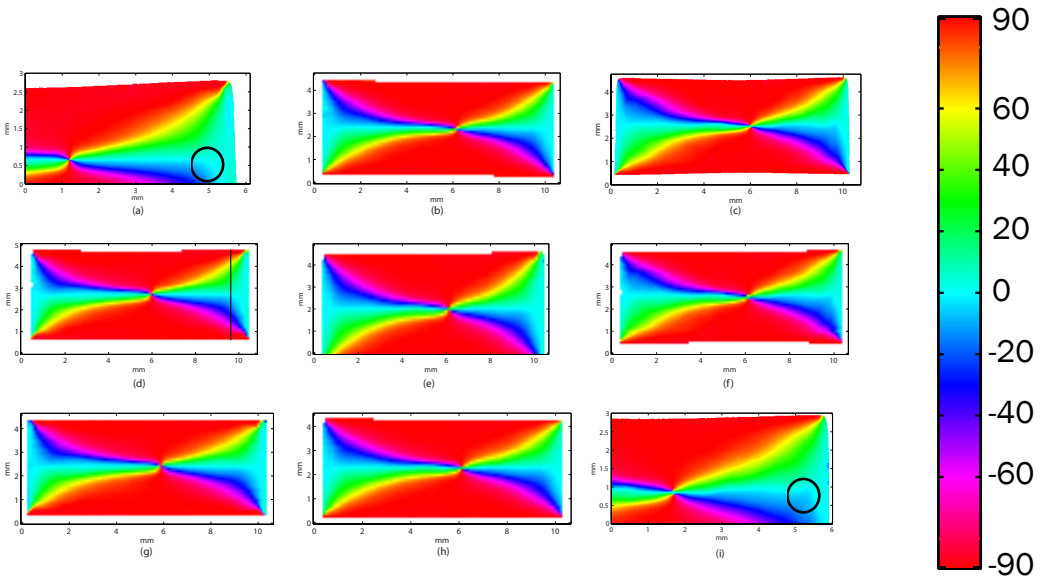

Figure 5.15: Development of orientation as function of shear rate and temperature for low q. Shear rate is increasing from left to right, temperature is increasing from top to bottom a) EDLL, b) EDLM, c) EDLH, d) EDML, e) EDMM, f) EDMH, g) EDHL, h) EDHM, i) EDHH. The color bar symbolizes the orientation of the diffraction peaks in degrees. The orientation of the diffraction pattern is clearly aligning itself perpendicular with the edges of the sample. Inside the black ring in figure (i) one can see a feature, where the dark blue orientation is turning slightly up. This is visible only for high shear rates, and only for one of the sides of the sample. One can not see this feature inside the black ring in figure (a), as one should expect, if this occurred for lower shear rates. The black line in figure (d) is indicating where the data for the 1D line plots in Figure 5.16 are taken from.

Figure 5.16 shows the orientation of the scattering signal through a single vertical line of the samples EDLL, EDLH, EDML, EDMH, EDHL and EDHH. It looks like the absolute value of the orientation is higher in the samples with low shear rate, compared to the samples with high shear rate, for the same temperature. When the temperature is rising, the difference in orientation seems to vanish. It is however a large uncertainty, as marked by the overlapping error bars.

Figure 5.17 shows the average orientation in the area marked with a black ring in Figure 5.15 (i) for six different sample types. The orientation looks to be lower for higher shear rates, but the difference is very small for high temperature. The uncertainty is also very high for the data taken from the low resolution scans, as can be seen by the large error bars, which form a 95 % interval of confidence for the true mean value of the orientation. It is therefor only the low temperature samples which can be said to be truly different with over 95 % probability. The samples produced under medium temperature also looks to be quite different, but this does

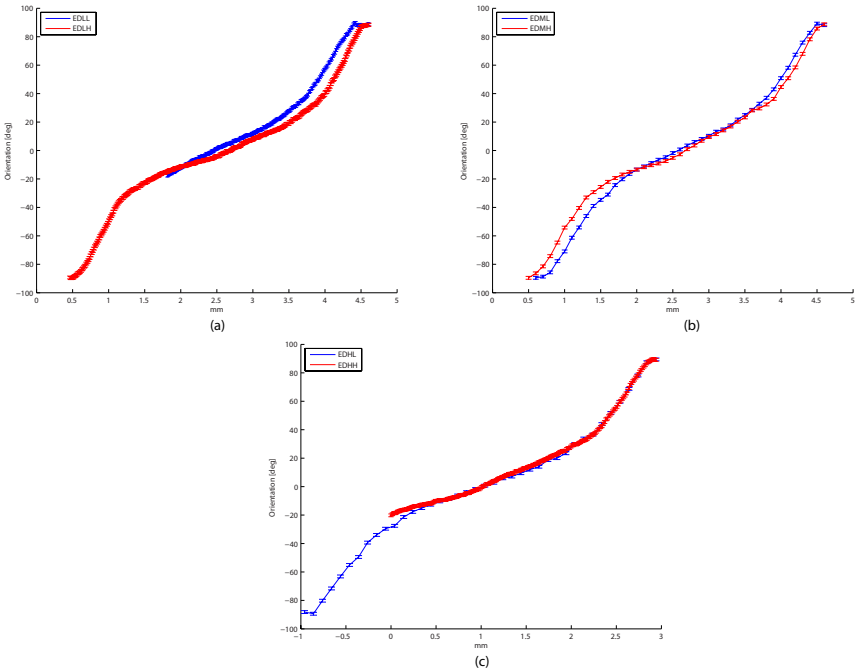

Figure 5.16: One-dimensional orientation plots of the SAXS data. (a) EDLL and EDLH, (b) EDML and EDMH, (c) EDHL and EDHH. The data is taken from roughly the same region on all the different samples. The orientation seem to have a tendency to be more aligned towards the top and bottom edge of the samples, as seen in figure (a) and (b), for lower shear rates, but that a higher temperature is equalizing this effect, as seen by the development of the differences between the curves, from (a) to (c).

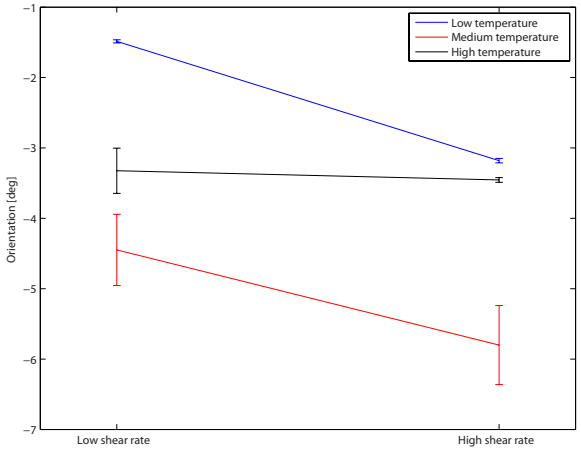

Figure 5.17: The mean value of the orientation in the area marked with the black ring in Figure 5.15 (i). The mean value of the orientation goes down for higher shear rates, but very little for high temperature. The sample number is however too low for the low resolution scans to say that they are different within a 95 % interval of confidence.

not have to be true, or the difference can be much smaller, since the error bars are overlapping.

Chapter 6

Discussion

6.1 Edge Effects on the Scattering Orientation

The figures in Chapter 5 shows that the scattering signal is strongly affected by the edges of the sample. The orientation prefers to align itself perpendicular to the edges, as seen in Figure 5.2, 5.4, 5.6, 5.8, 5.11 (a) and 5.12. All the plots of the cross section of the dog-bone show a significant sectioning of the sample, as seen in Figure 5.4 - 5.7. These figures indicate that it is possible to divide the sample into four regions; the top, bottom, left and right part that has the talc c-axis direction towards the edge, as indicated by Figure 6.1[1]. The fact that it is the c-axis of talc that has aligned itself comes from the fat that the diffraction peak of (006) was analyzed. This is consistent with the directional and visibility plots in Figure 5.2 and 5.3 which is of the front view of the dog bone neck. In this scan, the scattering vector will only be able to be equal the reciprocal lattice vector when it is not normal to the incoming wave vector, which is in area III and IV in Figure 6.1, and not in area I and II where the reciprocal lattice vector is parallel to the incoming wave vector. This can be visualized by looking at Figure 3.1 (b). In scan 109 the X-ray beam will see the reciprocal space as indicated in Figure 3.1 (b) in region III and IV, while in region I and II the X-ray beam will see a reciprocal space where the $\mathbf{x}^*$ and $\mathbf{z}^*$ axis is rotated 90°, without moving the incoming X-ray beam. The reciprocal lattice points can then not intersect the Ewald sphere and no scattering will occur. The visibility becomes lower towards the center because the X-ray beam travels through less material where the scattering condition can be fulfilled. At the very edge, the X-ray beam travels through almost only a volume with the reciprocal lattice vector in the correct direction to allow scattering, while closer to the center, a large part of the path the X-ray beam transverse is through section I and II, thus not contributing to the scattering. This is indicated in Figure 6.1. The visibility, which is an indication of degree of orientation, will therefore seem lower towards the center of the sample, because a large part of the orientation of the sample will not have a reciprocal lattice vector which fulfills the scattering conditions compared to the edges.

An interesting thing to notice is that the scattering peak is not symmetric, as is visible in Figure 5.1 (a). This was visible for all images from the cross section scans. This means that the c-axis is not perfectly aligned towards the edge, but is slightly

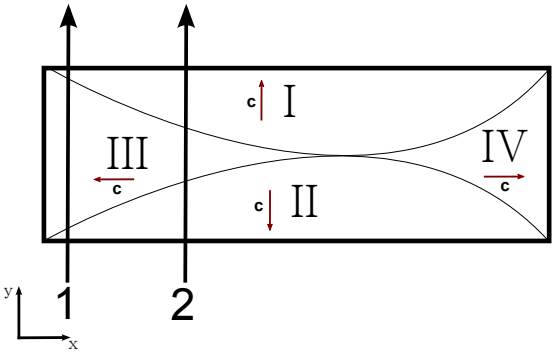

Figure 6.1: The areas of the cross section of the dog bone can be sectioned in to four different areas based on the direction of the scattering pattern. The direction of the talc c-axis is indicated in the figure. The two black lines symbolize the path the X-ray beam is traveling when the dog-bone is being scanned from the front (scan 109). As one can see, line 1 travels through a large part where the talc c-axis points to the right, while much of the distance line 2 travels through goes through area I and II, where the c-axis points along the beam, thus making it impossible to fulfill the scattering condition.

tilted. This can be explained by using the Ewald sphere in Figure 6.2. If the preferred direction of the c-axis of talc had been perpendicular to the surface edge, then the incoming beam would be directed normal on the c-axis, and the situation would be similar to the situation in Figure 6.2 (a). The scattering marked by the $\mathbf{k}_o$ would then apply and the scattered intensity would be equal, because the Ewald sphere intersect equal amount of the reciprocal lattice. If however the talc c-axis is slightly tilted, then the reciprocal lattice would be slightly tilted compared to the incoming beam, as illustrated in Figure 6.2 (b). The scattering for the top and bottom reflection would be of different intensity because a different volume of the reciprocal lattice would intersect the Ewald sphere. Since the image in Figure 5.1 (a) is taken from the cross section of the dog-bone neck, this implies that the preferred direction of the c-axis of talc is tilted slightly out of the cross section, which means in the flow direction of the injected polypropylene. In Figure 5.1 (b) the diffraction pattern is slightly tilted counter clockwise. The two peaks are in this image of almost similar intensity. This image is from scan 109, and it fits good with the assumption that the talc c-axis is tilted in the flow direction. When comparing the orientation in Figure 5.2 and visibility in Figure 5.3 of the dog-bone neck with the orientation in Figure 5.8 and the visibility in Figure 5.10 it makes it plausible that the orientation of the c-axis is the same in the house as the dog-bone, because the development of the visibility and orientation is very similar between the front scan of the dog-bone and all the scans of the house. The preferred direction of the c-axis of talc is hence towards the edges, with similar sections of the cross sections as in Figure 6.1 for the house as for the dog-bone. When looking close to the center of the house, almost none of the molecules will have a direction that can fulfill the scattering conditions, therefore the visibility will be very low towards the center, as seen in Figure 5.10, 5.11 (b) and 5.13. This can however not be fully verified without doing a measurement of the cross section of the house sample.

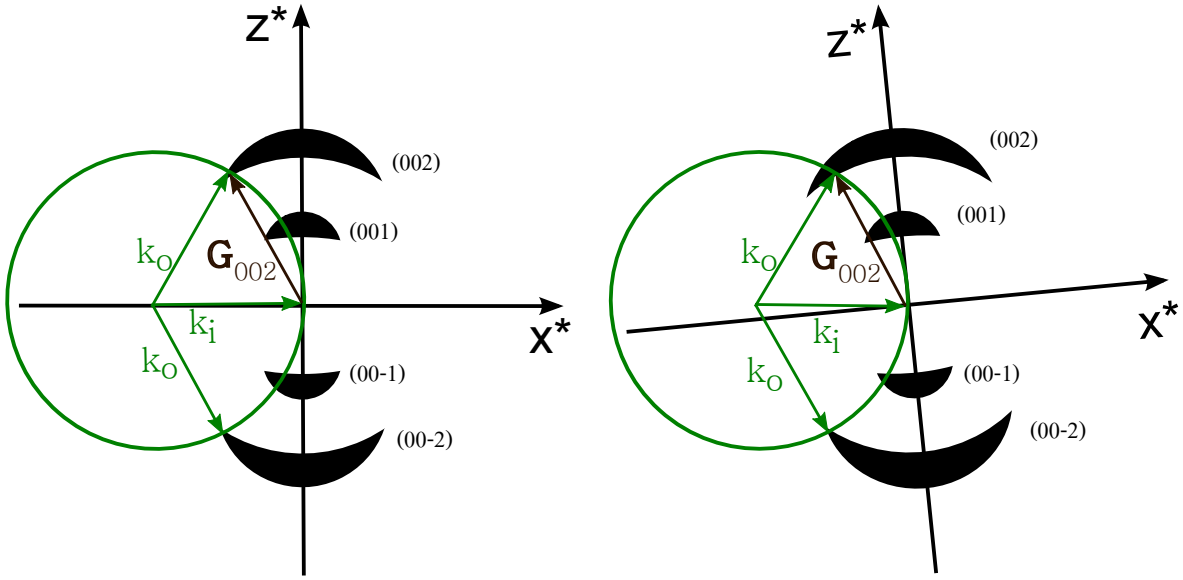

Figure 6.2: a) The Ewald sphere in reciprocal space where one of the axis in the reciprocal lattice is perpendicular to the incoming wave vector $\mathbf{k}_i$. The Ewald sphere intersect equal amount of the smeared out reciprocal point (002) as (00-2), and the scattering will therefor be equal in intensity. b) The Ewald sphere in reciprocal space where the incoming wave vector is not perpendicular to one of the reciprocal axis. The Ewald sphere is not intersecting equally much of the smeared out reciprocal points, and the scattering signal will therefor not have the same intensity.

The effect the edges has on the orientation is especially visible Figure 5.11. The transition from high thickness to low thickness at 8.5 mm and 13 mm in the vertical direction shows that any kind of edge will strongly affect the orientation of the crystalline material. In this figure, the visibility is high further in in the thick part of the sample compared to the thin part. This makes sense because with a smaller thickness, then area I in Figure 6.1 would need to be smaller because the thickness becomes thinner and the talc c-axis is turning quicker towards the other edges.

6.2 Decentering of orientation symmetry

From Figure 5.2 and 5.6 it is seen that the orientation is not symmetric around the center of the sample. It can be hypothesized that this is caused by the manufacturing procedure. The dog-bone is manufactured by injecting melted polypropylene at one of the sides. This flow can cause the shift in alignment of the symmetry of the orientation compared to the sample center. This effect can also be caused by the temperature gradient across the sample. During the manufacturing of the samples, one side of the dog-bone will have a slightly higher temperature than the other side. This difference in temperature across the sample can cause different

parts of the sample to crystallize at different times. The shifting of this alignment can be believed to cause some mechanical effects, although this has not been tested. To see what kind of mechanical effects this could have, it would be needed to make different samples, under different conditions. It is not known if the house sample also show this decentering of orientation and visibility symmetry compared to the geometrical symmetry. Testing how the injection and temperature gradient affect the sample could be done by varying those parameters, and measure how the symmetry is changing.

Also other effects on the samples can come from how the samples were made. In Figure 5.10 it was seen a thin layer of lower visibility near the bottom. This coincided with where it was a discontinuity in the horizontal orientation gradient, as shown in Figure 5.9. At the two bottom corners of the house sample, on could see that the talc c-axis did not align itself perpendicular with the edge, but parallel. This is also something that is most likely caused by how the polypropylene flows into the mold. In addition the visibility in Figure 5.3 and 5.5 shows that the degree of orientation between the upper, lower, right and left part varies also in the cross section of the dog-bone, although not in a major way. All these effects could be caused by the manufacturing procedure itself. If this is the case, then it should be possible to alter the different areas with respect to each other.

6.3 Effect on Mechanical Breaking of the Sample

In Figure 5.12 and 5.13 the effect of breaking off the polypropylene sample from the injection mold is shown. From Figure 5.12 it can appear like one of the molecular c-axis will align itself parallel to the breaking edge, but that some parts along the breaking edge has to have the molecular axes directed perpendicular to the edge. One reason for this alignment could be that the area of where the polypropylene was injected to the mold will have a strong directional alignment in the flow direction. This can be justified by the fact that around the breaking point all the directions seem to flow upwards. This flow seems to affect the direction at the center of the sample, which is tilted slightly upwards to the right. Another reason for this alignment around the breaking point could be caused by the physical breaking itself. When the sample is removed from the injection mold, the breaking of the sample will cause the molecules to turn and be broken off in such a way as to align itself along the edge. If this is the case, then it could be possible to manipulate the orientation around macroscopic areas by in some ways altering the sample physically.

As seen in Figure 5.13, the visibility is higher around the breaking edge. The breaking edge seems to go quite far in to the sample. It is thus likely that this high visibility is directly caused by the breaking, and not just because the breaking edge is close to where the polypropylene was injected, and the degree of orientation is just a result of the closeness to the injection. In all other measurements, the visibility drops off quite fast towards the center of the sample, and it is unlikely that the visibility would stay as high as it is at the breaking edge 2 mm towards the center from the edge. To see more of what could cause the effect of the alignment along

the breaking edge, it would be needed to be made measurements on samples with a cleaner breaking edge, and also with a breaking edge that does not go as deep as the one in this sample.

It can be speculated that the talc c-axis is not the reason for the alignment. It could well be one of the axes of polypropylene that align itself, and this drags the c-axis with it. It could be believed that the axis along the long chain of polypropylene will align itself along the cut edge. This could then position the c-axis of talc in such a way that it in some places will align itself parallel to the edge, and some places normal to the edge. To further analyze what happens at the edge, it would be needed to see how the axes of polypropylene behaves close to the edge.

6.4 Image Artifacts

In many of the figures one can see some pixels with a completely different value compared to the surroundings. This is for example visible in Figure 5.11 (b) where there are some dark red pixels close to the bottom of the figure. Also Figure 5.2 show some pixels with a bright yellow color, compared to the dark regions around, at roughly 7.5 mm in horizontal direction. This could be caused by the fact that the scattering peaks are very low, making it hard for the plotting routine to fit a correct curve to the data set, since the peaks are low compared to the background, and fluctuations in the background could be registered as a peak. The bright yellow pixels coincide with the pixels with high visibility at the center of the sample in Figure 5.3. This sudden rise in visibility seems unlikely when one considers the surroundings, and it was not observed any sudden rise in scattering intensity at the center of the sample from the images from the detector. It is therefore likely that the fitting routine failed in these pixels, due to the low scattering peaks.

6.5 Small-Angle X-ray Scattering

Figure 5.15 shows that the general tendency for all the different ED-samples are very similar with eachother. The alignment of the scattering pattern is perpendicular to the edges of the sample. This is also very similar to what was observed for the wide-angle X-ray scattering experiment. The samples measured contained a lot of talc. The scattered signal is therefore strongly influenced by these talc particles.

The feature which is marked by a black circle in Figure 5.15 (i) indicates that the shear rate has influence on the orientation of the scattering signal. Since this feature is seen on only one of the sides for high shear rates, it is plausible that it is partially caused by asymmetry in the injection of the polypropylene to the sample.

The orientations shown in Figure 5.16 shows that the scattering signal is more directed towards the top and bottom edge for lower shear rates, but that an increasing temperature is equalizing this difference. It could be speculated that a higher shear rate makes it harder for the molecules to be ordered towards the top and bottom edge, but that at higher temperature the movement of the molecules makes

it possible to align themselves. It is however a fairly large uncertainty in this, as shown by many of the overlapping error bars. The error bars have been calculated by accounting for the fact that each pixel has a finite size and that random fluctuation in the registered number of photons on each pixel could let a pixel report a higher count than its neighbor although this is false. The count rate was fairly high, so it was estimated that it would be unlikely that random fluctuations would cause a report of a false largest number of counts more than one pixel away from the largest value. From Figure 5.17 it is seen that the average orientation of the scattering signal is decreasing with higher shear rate. It is however only for the low temperature that it is enough data to have any statistical difference between low and high shear rate. It has here been approximated that the orientation will follow a t-distribution. This is strictly not entirely correct. The samples, each orientation, the mean is calculated from is not drawn from the same same probability distribution, and they don't have the exact same expected value for the orientation, since they naturally will align themselves to the wall, as seen in Figure 5.15. Thus the t-distribution is not directly applicable, since this should strictly only be used to finding the error estimate for a mean from samples drawn from the exact same probability distribution. The area which were analyzed showed however no abrupt change in orientation, and the expected value of the orientation in the analyzed region is therefore not too different, and therefore the t-distribution is used as an approximation for finding the uncertainty. To this approximation the observed difference in mean of the orientation could be caused by statistical fluctuations for the samples produces under medium and high temperature. The error estimate is rather large because of the low resolution of the scan causing only a few measurement to be the basis of the mean. The high resolution scan has however so many measurements of the analyzed region that the central limit theorem can be applied. This makes the t-distribution a better approximation and the standard deviation smaller. To be certain that the regions for medium and high temperature are different, high resolution scans should be taken of the relevant area, to get more data.

Chapter 7

Conclusion

It has been shown that the talc particles in injection molded isotactic polypropylene will align itself with its c-axis almost perpendicular to the edges, but with a small tilt in the flow direction. It is also shown that any kind of edge will have a strong effect on the alignment, either the edge of the sample itself, or internal edges separating different thicknesses. This effect is verified for a sample shaped as a dog-bone, but it is also likely that this will occur for other shapes, like a house. This analysis covered however only talc, and did not look more at the scattering from polypropylene.

The scattering signal from the small angle X-ray scattering experiment of the different talc filled iPP samples manufactured under different conditions shows alignment parallel to the surface normal. It was also discovered that different shear rates and temperatures have implications on the orientation. A high shear rate would form a peninsula in orientation compared to the surroundings, but only for one of the sides. It was clearly a difference in the average orientation of this area for the different temperatures. The orientation for different shear rates of the high and medium temperature showed no significant statistical difference due to the lack of data. It can however look like the difference in the average orientation between low and high shear rate is lower for samples made under high temperatures, compared to the samples made under low and medium temperatures. The samples manufactured with low shear rate seemed to have a scattering pattern aligned more towards the top and bottom part of the sample, compared to the samples manufactured with high shear rate, when looking at the vertical direction. This difference becomes smaller with increasing temperature, but the rather overlapping error bars makes this conclusion rather uncertain. It is not yet clear what direct implications this has on the internal structure, but encourage further studies on the sample since it shows directional alignment, and can therefore possibly be related to the alignment shown in the WAXS regime.

The production method also seem to influence the symmetry of the orientation of the sample, since this is not symmetric compared to the center of the sample. Effects as a temperature gradient across the mold and the way the melted polypropylene will enter the mold can be reasons for this effect, and a continued study on these effects could give answers to why the misalignment occurs, and what kind of mechanical effects this has on the sample. A thin layer of lower visibility formed in the sample

shaped as a house between the lower edge and the interior which coincide with a discontinuity in the horizontal gradient of the orientation development. This discontinuity is not yet understood, but a further analysis of the flow of the polypropylene in to the mold could give an explanation to this.

It is also seen that mechanically breaking the sample will have large implications on the orientation of the c-axis to talc. The orientation and visibility is much stronger along the edge. The exact reason for this is unknown, but with further studies one can perhaps find a way of manipulate the direction of the crystalline axis close to the surface by mechanically altering the macroscopic sample.

Bibliography

[1] H. Granlund, J. B. Fløystad, M. Esmaeili, E. T. Bakken, M. Bech, P. E. Vullum, E. Andreassen, and D. W. Breiby, "Mapping structural gradients in isotactic polypropylene using scanning wide-angle x-ray scattering," *Polymer*, vol. 54, no. 7, pp. 1867 – 1875, 2013. Available Online.

[2] C. M. I. Consulting, "Market study: Polypropylene," 2012. Available online.

[3] R. Kongsmo, "Prosjektrapport," Master's thesis, Norwegian University of Science and Technology, 2012.

[4] F. P. van der Burgt, *Crystallization of isotactic polypropylene The influence of stereo-defects*. PhD thesis, Technische Universiteit Eindhoven, 2002. ISBN 90-386-2674-6.

[5] "Wikipedia: polypropylene." http://en.wikipedia.org/wiki/Polypropylene.

[6] M. A. G. C. Marco, G. Ellis and J. M. Arribas, "Analysis of the dynamic crystallisation of isotactic polypropylene/α-nucleating agent systems by dsc," *Thermal Analysis and Calorimetry*, vol. 68, pp. 61–74, 2002. Available online.

[7] S. Z. D. Cheng, J. J. Janimak, and J. Rodriguez, "Crystalline structures of polypropylene homo- and copolymers," *Polypropylene: Structure, blends and composites*, vol. 1, pp. 31–52, 1995. Available online.

[8] F. Khoury, "The spherulitic crystallization of isotactic polypropylene from solution: On the evolution of monoclinic spherulites from dendritic chain-folded crystal precursors1," *JOURNAL OF RESEARCH of the National Bureau of Standards -A Physics and Chemistry*, vol. 70A, no. 1, 1966. Available online.

[9] Y. Wang, C. Chen, J.-Z. Xu, J. Lei, Y. Mao, Z.-M. Li, and B. S. Hsiao, "Suppressing of γ-crystal formation in metallocene-based isotactic polypropylene during isothermal crystallization under shear flow," *The Journal of Physical Chemistry B*, vol. 116, no. 16, pp. 5056–5063, 2012. Available online.

[10] R. H. Todd, D. K. Allen, and L. Alting, *Manufacturing Processes Reference Guide*. Industrial Press Inc, first ed., 1994.

[11] R. A. Phillips and M. D. Wolkowicz, *Polypropylene Handbook*. Hanser, 2005.

[12] B. E. A. Saleh and M. C. Teich, *Fundamentals of photonics*. Wiley, second ed., 2007.

[13] D. J. Griffiths, *Introduction to electrodynamics*. Pearson, third ed., 2008.

[14] J. Als-Nilsen and D. McMorrow, *Elements of modern x-ray physics*. Wiley, second ed., 2010.

[15] C. Kittel, *Introduction to Solid State Physics*. Wiley, eighth ed., 2005.

[16] Walpole, Myers, Myers, and Ye, *Probability & Statistics for Engineers & Scientists*. Pearson Education, eighth ed., 2007.

[17] http://www.psi.ch/sls.